Substitutionally rhodium(IV)-doped titania showing photocatalytic activity toward organics oxidation under visible-light irradiation

Shubin Yang[a*], Bunsho Ohtani[b]

[a]School of Chemistry and Chemical Engineering, Yantai University, Yantai 264005, P.R. China

[b]Institute for Catalysis, Hokkaido University, Sapporo 001-0021, Japan

Keywords: titania, rhodium(IV) doping, photocatalysis, visible-light irradiation

ABSTRACT

In this study, an aqueous solution containing rhodium(IV) (Rh(IV)) was prepared by oxidation of rhodium(III) (Rh(III)) with solid sodium bismuthate in nitric acid and then used as a medium for hydrothermal titania preparation to obtain rhodium-doped titania (Rh-TiO_2) composite. Rh(IV) species were observed in Rh-TiO_2 in XPS analysis. Effect of rhodium/titanium molar ratio (Rh/Ti) on the photocatalytic activity was studied. The obtained characteristics suggest successful rhodium substitution and doping of titania to give visible-light absorption. The Rh-TiO_2 composite exhibits enhanced photocatalytic activity for acetic acid decomposition and 2-propanol oxidation under UV-visible (> 290 nm) and visible-light (> 450 nm) irradiation, respectively. The enhanced photocatalytic activity is attributable to the visible-light absorption induced by rhodium doping. These results indicate that Rh-TiO_2 photocatalyst materials could be promising materials for high-efficiency photooxidation reactions under visible-light irradiation.

1. Introduction

With the rapid increase industrialization in many countries, the pollution load on the environment is increasing [1-3]. The significant rise in photocatalysis due to the increasingly serious environmental issues has generated worldwide concern. Photocatalysis is an environmentally friendly technology to covert solar energy into chemical energy for the promising

applications of the photoredox reactions of target organic matters [4, 5]. In recent decades, photocatalysis research has mainly focused on water splitting, carbon-dioxide reduction, degradation of organic pollutants, air remediation and self-decontaminating surfaces [6, 7]. Various semiconductors including oxides, sulfides, and nitrides have been explored as possible photocatalysts in past decades [8]. Up to now, titanium(IV) oxide (TiO_2) has been one of the most promising photocatalysts because of its easy availability, low toxicity, high photostability, and high efficiency. However, the application of pure TiO_2 is limited, because it requires ultraviolet light (bandgap: ~3.0eV), which makes up only a small fraction (< 4%) of the total solar spectrum reaching the surface of earth. Therefore, the development of efficient photocatalysts with visible light has become an important research direction. The doping of TiO_2 with metallic and nonmetallic elemental creates localized/delocalized states in the band gap, which extends its optical absorption to the visible region [9]. Therefore, doping is deemed to be a promising approach to improve the utilization rate of solar energy for TiO_2.

Rhodium (Rh)-doped titania and/or strontium titanate ($SrTiO_3$) photocatalysts have attracted considerable scientific interest for their high photocatalytic properties under visible-light irradiation. Kudo's group published a series of papers on rhodium-doped strontium titanate and showed that Rh-doped $SrTiO_3$ is a potentially useful visible-light water-splitting photocatalyst [10-12]. In our previous study, we found that Rh-doped TiO_2 exhibits high photoelectrochemical properties under visible-light irradiation via a two-photon band-gap excitation mechanism [13-15]. One of the reasons of the high-level activities is possible substitution of titanium(IV) with rhodium(IV) (Rh(IV)) in crystalline lattice owing to their same charge and coordination as well as to their very closed ion size. However for the efficient substitution it is necessary to oxidize Rh(III) in available precursors before or during a doping process [13-15].

In the present study, we tried to dope Rh(IV) ions directly into the framework of TiO_2 nanosheets by a novel hydrothermal method. In order to understand the valence state of rhodium in the Rh-TiO_2 composite, the element characterization of Rh-TiO_2 composite will be accurately analyzed by XPS. In the experiment, transparent substrates in the region of working wavelengths,

such as acetic acid and 2-propanol, is used in the photocatalytic-activity test for photocatalysts and for action spectrum analysis. The photocatalytic activities of the Rh-TiO_2 materials is studied by the photocatalytic decomposition of acetic acid under UV-light irradiation and the photocatalytic oxidation of 2-propanol in water under visible-light irradiation (> 450 nm). The effect of Rh/Ti molar ratio on the photocatalytic activity is also studied. The photocatalytic activities of Rh-TiO_2 materials is evaluated with bare TiO_2 as a reference.

2. Materials and methods

2.1. Preparation of Rh-TiO_2

2.1.1 Rh(III) oxidization

The Rh-TiO_2 composite was prepared via three successive processes: Rh(III) oxidization, a hydrothermal process and an acidolysis treatment. In a typical reaction, 2 mol L^{-1} nitric acid (HNO_3), 0.1 mol L^{-1} rhodium(III) chloride trihydrate ($RhCl_3 \cdot 3H_2O$) and solid sodium bismuthate were sequentially added to a conical flask. After reaction for 20 h under constant stirring at ambient temperature, the purple Rh(IV) solution (0.0025 mol L^{-1}), as a precursor solution, was collected by centrifugation (4000 rpm, 5 min). The prepared Rh(IV) species can be detected spectrophotometrically using the absorption band at 550 nm on a MPS-2450 UV-Visible Spectrophotometer (Shimadzu, Japan).

2.1.2. Hydrothermal process

After collection of the Rh(IV) solution, a 4-mL portion of tetrabutyl orthotitanate was added dropwise to 34-mL Milli-Q water under continuous stirring for 30 min. After the hydrolysis reaction, 10 mL of the prepared Rh(IV) solution was injected under stirring for 10 min. Then, the colloidal solution was transferred into a 100-mL Teflon-lined stainless-steel autoclave and kept at 453 K for 10 h. After the hydrothermal reaction, the gray precipitates were collected by centrifugation, washed with water and alcohol, and dried in a vacuum oven at 353 K.

2.1.3. Acidolysis treatment

To remove bismuth species, the obtained gray precipitates was redissolved in concentrated nitric acid under continuous stirring for 3 d. Finally, the Rh-TiO_2 composites were obtained by centrifugation, washed with water, and dried in a vacuum oven. Rh-TiO_2 composites with different rhodium/titanium molar ratios (0 - 2.0% Rh/Ti) were prepared.

2.2. Characterizations

The synthesized Rh-TiO_2 composites were characterized using different techniques. The DRS spectra were monitored by a JASCO V-670 spectrophotometer. The SEM images were obtained with a Shimada JSM-7400F spectroscope. The XPS analysis was carried out on Thermo ESCALAB 250 electron spectrometer to analyze the valence state of rhodium in Rh-TiO_2.

2.3. Photocatalytic activity test

The photocatalytic activities of the obtained samples under ultraviolet-light and visible-light (UV-Vis, >290 nm) irradiation were evaluated by photocatalytic decomposition of acetic acid. 5 mL of 5vol% acetic-acid solution was added to a borosilicate glass test tube, which contained 50 mg of a photocatalyst. The prepared suspension was irradiated (> 290 nm) with a 400-W high-pressure mercury lamp (Eiko-sha) at 298 K under magnetic string (1000 rpm). The liberated carbon dioxide (CO_2) was monitored by a gas chromatograph (TCD-GC). The irradiation was performed until an almost linear increase in the CO_2 amount was observed. Rh-TiO_2 with different doping levels were compared to evaluate the photocatalytic activity of the Rh-TiO_2 photocatalysts.

The photocatalytic activities of the obtained samples under visible-light irradiation were evaluated by photocatalytic oxidation of 2-propanol in aqueous suspension. A 50-mg amount of photocatalyst was suspended in 5-mL 5vol% aqueous 2-propanol in a glass test tube and then sonicated for 30 s in the dark by shielding light with aluminum foil. Then, the suspension was irradiated under visible light with a xenon lamp and an optical cut-off filter (Y48; > 450 nm). Then, 0.5-mL suspension was filtrated with a 0.2-μm filter membrane, and the generated acetone in a 5-μL portion of the supernatant solution was analyzed by FID gas chromatography.

Action spectra were measured with monochromatic-light irradiation in the wavelength range from 300 to 630 nm using a diffraction grating-type illuminator (JASCO, CRM-FD) equipped with a 300 W xenon lamp (Hamamatsu Photonics, C2578-02). The light intensity at each wavelength was adjusted by stainless-steel mesh filters. The apparent quantum efficiency (QE) was measured under the same photocatalytic reaction conditions.

3. Results and discussion

3.1. The morphology and microstructures of Rh-TiO_2.

The morphology and microstructures of Rh-TiO_2 were characterized by SEM (**Fig. 1**). All the materials showed heavily aggregated small nanoparticles, resulting in a high rock-like macroparticle volume. After rhodium doping, a similar morphology was observed in the SEM images of the Rh-TiO_2 composites. Uniform nanoparticles aggregated and randomly decorated on the rough surface of the bulk particles. Rhodium exists homogeneously in 2% Rh-TiO_2, as observed by elemental mapping (**Fig.2**). X-Ray diffractometry showed that the crystalline phase of TiO_2 was anatase with negligible amount of brookite.

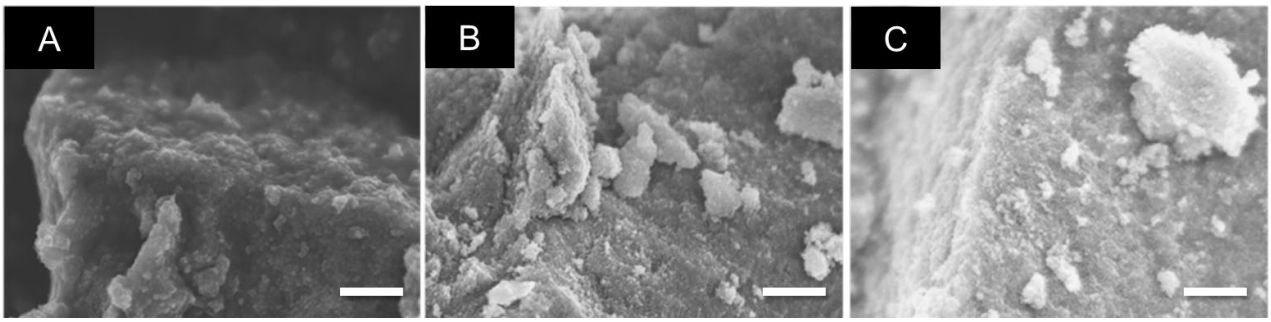

Fig. 1 SEM images of bare TiO_2 (A), 0.22% Rh-TiO_2 (B), and 2.0% Rh-TiO_2 (C). White bars correspond to 500 nm.

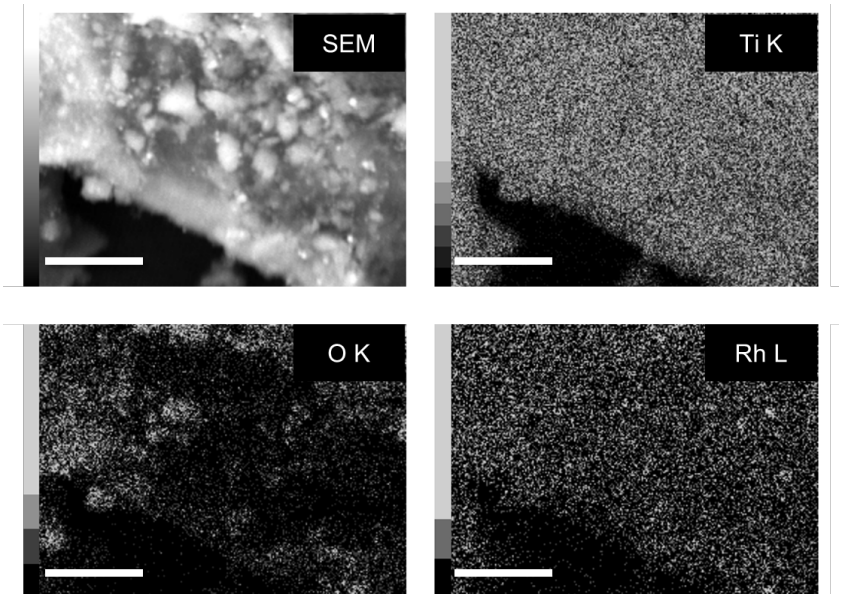

Fig. 2 SEM and EDX-mapping images of 2% Rh-TiO_2. White bars correspond to 5 μm.

3.2 The valence state of rhodium in Rh-TiO_2.

XPS analysis confirmed the absence of bismuth and the valence state of rhodium in the Rh-TiO_2 composites. No obvious peaks for bismuth were observed for Rh-TiO_2 composites, indicating that the bismuth ions were completely dissolved and removed from the composite by the above-mentioned strong acid treatment. The binding energies for Ti $2p_{3/2}$ and Ti $2p_{1/2}$ in **Fig. 3(A)** were observed at 458.5 ± 0.3 eV and 464.2 ± 0.1 eV, respectively, which are typical XPS peaks of Ti(IV) in TiO_2 [16, 17]. Moreover, no trace of Ti(III) or Ti(II) was found, Ti $2p_{3/2}$ peaks of which have been reported to be located at 457.6 eV and 456.4 eV, respectively [18]. The O 1s spectrum (**Fig. 3(B)**) can be fitted by three Gaussian components at 529.7, 531.8 and 533.3 eV. The binding energy at 529.7 eV can be assigned to the oxygen bound to Ti(IV) ions in TiO_2, while the binding energy located at 531.8 eV can be attributed to the oxygen deficiencies of TiO_2 [18]. The small shoulder at 533.3 eV related to the existence of hydroxide (-OH) groups [18, 19]. The traces of Rh were observed in 2% Rh-TiO_2 by XPS, as shown in **Fig. 3D**. The two intense peaks at 310.8 eV and 306.7 eV are assigned to Rh $3d_{5/2}$ and Rh $3d_{3/2}$, respectively. This indicates that

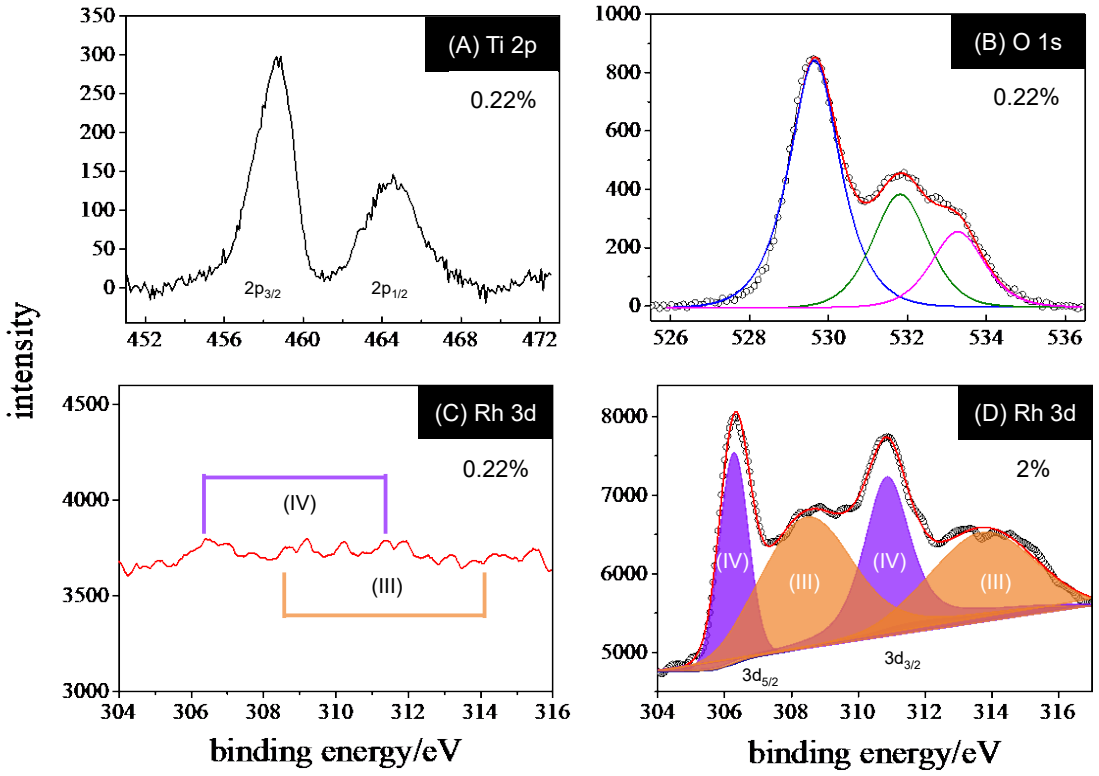

Fig. 3. Ti 2p (A), O 1s (B) and Rh 3d (C and D) XPS spectra of the obtained Rh-TiO_2 composites.

the Rh^{4+} valence state was in the final composites [12, 20]. In addition, two peaks at 313.4 eV and 308.9 eV were also observed in **Fig. 3D**, indicating that the Rh(III) valence state was also present in the 2% Rh-TiO_2 composite [10]. The Rh(IV) content in the 2% Rh-TiO_2 composite is higher that of Rh(III), the ratio is estimated to be 1.38:1. The lower-energy side Rh(IV) and Rh(III) peak could also be seen in the spectrum for 0.22% Rh-TiO_2 (**Fig 3(C)**). These facts suggests that Rh(IV) successfully substitutes with Ti(IV) in the crystalline lattice due to the very similar ionic radii of Rh(IV) (0.600 Å) and Ti(IV) ions (0.605 Å) especially in low-doped (0.22%) Rh-TiO_2 and high-doped Rh-TiO_2 might contain rhodium(III) oxide deposits on the surface as well as substitutionally doped Rh(IV) in the crystalline lattice. Although rhodium-modified or rhodium-doped materials have been widely studied [12, 15, 21-24], only Rh(III) or binary Rh(III) and Rh(IV) valence states coexist in these materials and no evidence to exclude the possibility of

inclusion of rhodium in the surface deposits; TiO_2 directly doped with the Rh(IV) valence state has not been reported. This may be the first report of true substitutional rhodium doping of titania.

Further proof was obtained by XRD. After rhodium doped, the (110) reflection of anatase shifted gradually from 25.43° to 25.30° with higher Rh concentrations (**Fig. 4A**), implying the rhodium is included in the crystal lattice. This is because the Rh(IV) ion has the same charge and coordination as well as the very closed ion size with Ti(IV). Therefore, the XRD results confirmed the true synthesized substitutionally rhodium(IV)-doped titania.

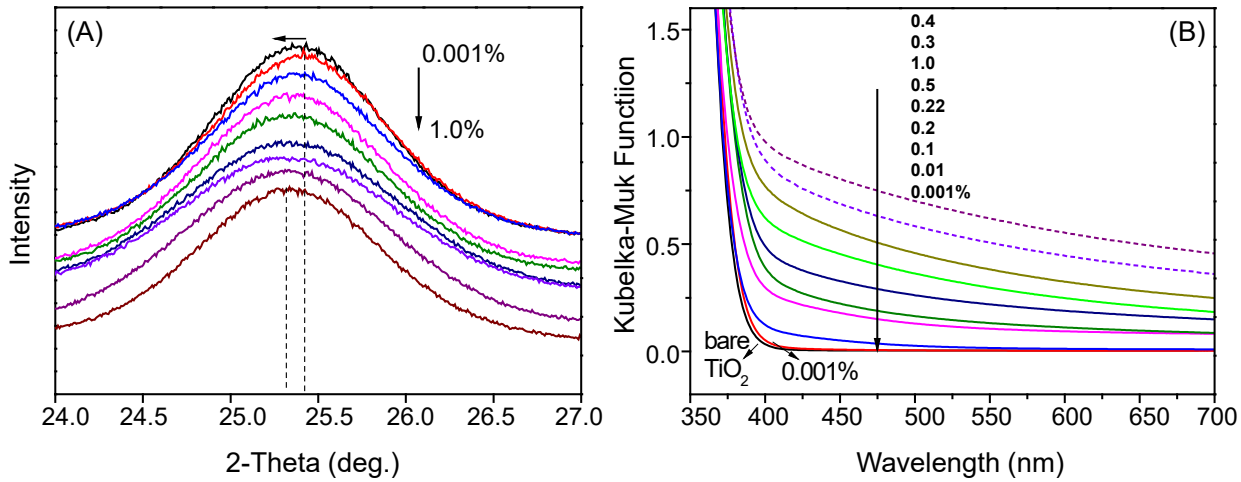

Fig. 4 XRD patterns (A) and DRS spectra (B) of bare TiO_2 and Rh-TiO_2 composites.

3.3 The absorption bands of Rh-TiO_2.

Figure 4B shows the diffuse reflection (DRS) spectra (DRS) of the obtained samples containing 0.001—1.0mol% of Rh. The band gap of the powder samples was calculated by the Kubelka–Munk method [15]. The approximate cut-off wavelength and band gap of bare TiO_2 and the Rh-TiO_2 composites are listed in **Table 1**. A reference sample (bare TiO_2) prepared by the same hydrothermal method was studied. The bare TiO_2 absorption spectrum exhibited an absorption edge at approximately 394 nm, assignable to the electron transition from the valence band composed of O_{2p} orbitals to the conduction band consisting of the empty 3d orbitals of Ti [25, 26]. For this bare TiO_2 sample, the main absorption within the visible range of light can be

Table 1 The absorption-edge wavelength and calculated bandgap of bare TiO_2 and Rh-TiO_2 samples.

Sample	bandgap/eV	absorption edge/nm
bare TiO_2	3.15	394
0.001% Rh-TiO_2	3.14	395
0.01% Rh-TiO_2	3.12	397
0.1% Rh-TiO_2	3.10	400
0.2% Rh-TiO_2	3.02	410
0.22% Rh-TiO_2	3.01	412
0.3% Rh-TiO_2	2.94	422
0.4% Rh-TiO_2	2.92	425
0.5% Rh-TiO_2	3.02	410
1.0% Rh-TiO_2	2.99	415

ignored. In contrast, Rh-TiO_2 samples (**Fig. 4B**) show broader absorption bands in the visible-light region (ca. 400-700 nm) than the original band gap transition of the host TiO_2 (< 400 nm). This is consistent with previous reports[11, 12, 22] that doped Rh species in metal oxides such as $SrTiO_3$ and TiO_2 exhibit a broad absorption band in visible-light wavelength region that extends to far infrared wavelengths.

The absorption in the visible-light absorption bands of Rh-TiO_2 became higher with the Rh concentration. In particular, 0.3% Rh-TiO_2 and 0.4% Rh-TiO_2 exhibited stronger absorption than the others. The bandgaps[27] of 0.3% Rh-TiO_2 and 0.4% Rh-TiO_2 are 2.94 and 2.92 eV (Table 1), respectively. This is consistent with the powder color changes of the Rh-TiO_2 samples, as shown in **Fig.5**. From 0.4% Rh-TiO_2, increases of Rh content caused surface states weakly absorbing within visible range of light, due to the coverage of excess rhodium (oxide) deposits inhibiting photoabsorption.

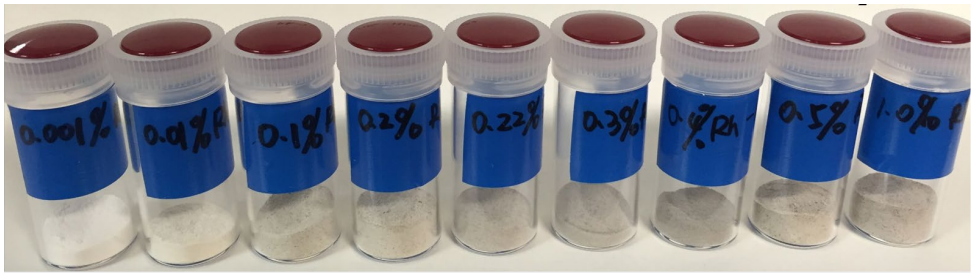

Fig. 5 Color differences of obtained Rh-TiO_2 powders.

3.4 Visible-light photocatalytic activity

The photocatalytic oxidative decomposition of acetic acid was studied to evaluate the photocatalytic activity of this novel Rh-TiO_2 composites. The rate of CO_2-generation by Rh-TiO_2 was deduced from the linear fitting of the volume of CO_2 with illumination time, as shown in **Fig. 6A**. Compared with bare TiO_2, all the Rh-TiO_2 composites exhibited better photocatalytic activity for the oxidative decomposition of acetic acid (**Fig. 6B**), indicating that the doping of Rh could enhance the photocatalytic activity for the decomposition of acetic acid. Especially, an extremely small amount of Rh (0.001%) could give titania an enhanced photocatalytic activity. With the increasing Rh doping level ($\leq$ 0.22%), the oxidation ability of the Rh-TiO_2 material increases, which may correspond to the broader and enhanced absorption band (**Fig. 4B**). The best loading amount of rhodium was 0.22 mol% with a CO_2 yield of 98.6 μmol h^{-1}. It can be calculated that the rate of CO_2 liberation by 0.22% Rh-TiO_2 is approximately 3.2 times higher than that of bare TiO_2 (**Fig. 6(A)**). However, excessive doping of Rh caused progressive deactivation of the Rh-TiO_2 composites, which might be due to enhanced recombination with rhodium species [15, 28] to coverage of excess rhodium (oxide) deposits inhibiting photoabsorption and/or recombination acceleration. This is in agreement with previous studies [15, 29] showing that a higher content of Rh in titania will have a negative effect on the photocatalytic activity. The enhanced photocatalytic activity of CO_2 production by the Rh-TiO_2 photocatalyst was due to the addition of Rh species, which may work as a cocatalyst for effective reduction of molecular oxygen, the counter reaction of acetic-acid oxidation. The addition of Rh species mainly substitutes with Ti(IV) in the

crystalline lattice especially in low-doped (0.22%) Rh-TiO_2 not disperses on the titania surface in the form of oxide clusters, and resulting in a smaller bandgap and an broader absorption in visible–light region (400 – 700 nm).

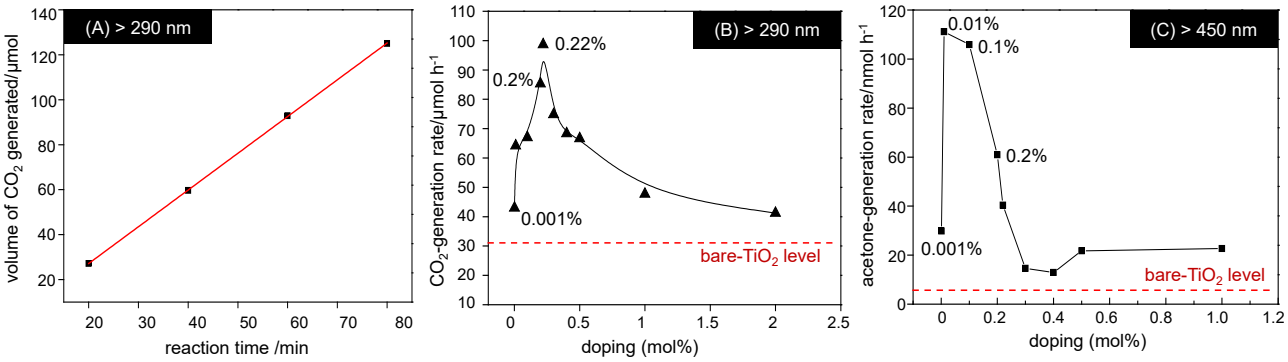

Fig. 6 Volume of CO_2 generated by 0.22% Rh-TiO_2 (A) and the rates of CO_2 (B) and acetone (C) production by Rh-TiO_2 composites with a series of rhodium doping levels under (B) UV and (C) visible irradiation.

The visible-light photocatalytic activity of Rh-TiO_2 was also studied for 2-propanol oxidation under aerobic conditions under visible-light (> 450 nm) irradiation. The photocatalytic activity of Rh-TiO_2 composites depends significantly on the rhodium doping level (**Fig. 6(C)**). In particular, the 0.01% Rh-TiO_2 sample shows the highest acetone generation rate, 111 nmol h-1, which is 20.5 times higher than that of bare TiO_2 (5.4 nmol h^{-1}). This is different from the photocatalytic degradation of acetic acid under UV-light irradiation, in which the 0.22% Rh-TiO_2 sample showed the highest CO_2-liberation rate. Compared with bare TiO_2, all the Rh-TiO_2 samples exhibited better photocatalytic activity, which is attributed to the enhanced absorption band in visible-light wavelength region that extends to far infrared wavelengths (**Fig.4B**). The excess doping at > 0.2mol% might induce inhibition of visible-light absorption of substitutionally doped rhodium by the possible surface-deposited rhodium oxides and/or enhanced recombination of photogenerated active species. All the Rh-TiO_2 composites exhibited better oxidation ability. Theoretically, titania could produce reactive oxygen species under UV irradiation, therefore, the enhanced oxidation ability of the Rh-TiO_2 material may related to the abundant generated reactive oxygen species

induced acetic acid and 2-propanol oxidation.

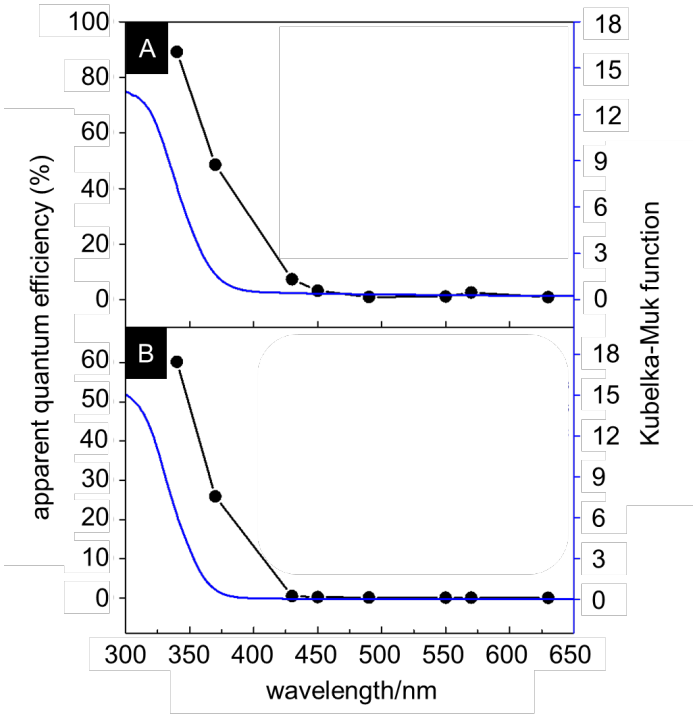

Fig. 7 Action spectra of the photolytic reactions of (A) acetic-acid decomposition (by 0.22% Rh-TiO_2) and (B) 2-propanol oxidation (by 0.01% Rh-TiO_2). The blue lines represent diffuse reflectance spectra of the

The action spectra of photocatalytic acetic acid decomposition (CO_2 evolution) and 2-propanol oxidation under aerated conditions were also observed. The apparent quantum efficiency (AQE) was calculated as the ratio of the rate of e^- (h^+) consumption to the flux of incident photons. **Fig. 7** shows the action spectra of the photocatalytic reactions of (A) and (B) irradiation at different wavelengths. From the above-mentioned experimental observations, the best loading amount of rhodium was found to be 0.22 mol% and 0.01 mol% for acetic acid decomposition and 2-propanol oxidation, respectively. Therefore, in the current study, we investigated the spectra over time for acetic acid decomposition (CO_2 evolution) and 2-propanol oxidation (acetone evolution) driven by the 0.22% Rh-TiO_2 and 0.01% Rh-TiO_2 samples, respectively. As shown in **Fig. 7**, the calculated AQE values at 450 nm for the 0.22% Rh-TiO_2 and 0.01% Rh-TiO_2 samples in reaction (A) and (B) are up to 3.3% and 0.2%, respectively. The AQE decreases with increasing

wavelength, indicating that both the CO_2 and acetone evolution relies on the light absorption property [30]. In addition, the observed spectral shape is similar to the corresponding diffuse reflectance spectrum, suggesting that Rh-TiO_2 could be used as a photocatalyst [26] at least under UV irradiation. In the visible-light range of spectra (B), AQE was negligibly small and any absorption feature could not be observed.

Based on these results and discussion, a possible photocatalytic mechanism of Rh-TiO_2 is that a new band is introduced between the valence band and conduction band of titana, which is supported by theoretical calculations[31, 32]. In addition, this new band in current research is supposed to be mainly composed of the 4d orbitals of Rh(IV). The transition from valence band of titana to the new band broadens absorption into visible–light region (400 – 700 nm) to generate more active oxygen species[33] to enhance the oxidation ability.

4. Conclusions

For the first time, titania which is directly doped with Rh(IV) was successfully synthesized by a hydrothermal treatment of suspension containing Rh(IV) species. The effect of the rhodium/titanium molar ratio on the photocatalytic activity was studied, and the obtained characteristics suggest successful substitutional doping of titania with Rh(IV) to give visible-light absorption. The results indicate that the Rh-doped titania composite exhibits enhanced photocatalytic activity for acetic acid decomposition and 2-propanol oxidation under UV-visible (> 290 nm) and visible-light (> 450 nm) irradiation, respectively. The enhanced activity is attributable to the wide range (ca. 400 – 700 nm) absorption induced by rhodium doping. These experimental observations indicate that rhodium doping could improve the utilization rate of solar energy for TiO_2 to enhance its photooxidation activity.

CRediT authorship contribution statement

Shubin Yang: Conceptualization, Visualization, Investigation, Writing.

Bunsho Ohtani: Supervision, Resources. Discussion, Writing.

Declaration of Competing Interest

The authors declare that they have no known competing financialinterests or personal relationships that could have appeared to influence the work reported in this paper.

Acknowledgements

Key Lab of Photovoltaic and Energy Conservation Materials (PECL2019KF014), Chinese Academy of Sciences is gratefully acknowledged by the authors.

Corresponding Author: Shubin Yang: shubinyang@ytu.edu.cn

References

[1] S. Yang;S. Liao;X. Ren;Y. Li;Y. Ma;Z. Zhang, Highly selective enrichment of radioactive cesium from solution by using zinc hexacyanoferrate(III)-functionalized magnetic bentonite, *J. Colloid Interface Sci.*, **2020**,580, 171-179.

[2] B. Ohtani, Hidden but Possibly Fatal Misconceptions in Photocatalysis Studies: A Short Critical Review, *Catalysts*, **2016**,6, 192.

[3] R.O.A. Rahman;H.A. Ibrahium;Y. Hung, Liquid Radioactive Wastes Treatment: A Review, *Water*, **2011**,3, 551-565.

[4] S. Yang;X. Du, Enhanced dispersion of carbon nanotubes in water by plasma induced graft poly(N,N-dimethylacrylamide) and its application in humic acid capture, *J. Mol. Liq.*, **2019**,277, 380-387.

[5] J. Shi;A. Wittstock;C. Mahr;M.M. Murshed;T.M.R. Gesing, A.; ;M. Bäumer, Nanoporous gold functionalized with praseodymia–titania mixed oxides as a stable catalyst for the water–gas shift reaction, *Phys. Chem. Chem. Phys.*, **2019**,21, 3278-3286.

[6] M. Zhao;H. Xu;H. Chen;S. Ouyang;N. Umezawa;D. Wang;J. Ye, Photocatalytic reactivity of {121} and {211} facets of brookite TiO_2 crystals, *J. Mater. Chem. A*, **2015**,3, 2331-2337.

[7] H. Hirakawa;M. Katayama;Y. Shiraishi;H. Sakamoto;K. Wang;B. Ohtani;S. Ichikawa;S. Tanaka;T. Hirai, One-pot synthesis of imines from nitroaromatics and alcohols by tandem photocatalytic and catalytic reactions on degussa (evonik) p25 titanium dioxide, *ACS Appl. Mater. Interfaces*, **2015**,7, 3797-3806.

[8] S. Zhang;J. Li;M. Zeng;J. Xu;X. Wang;W. Hu, Polymer nanodots of graphitic carbon nitride as effective fluorescent probes for the detection of Fe^{3+} and Cu^{2+} ions, *Nanoscale*, **2014**,6, 4157-4162.

[9] S.O. Sanni;O.G. Idemudia, Synthesis and Characterization of Rhodium Doped on TiO2/HCP for Enhanced Photocatalytic Performance on Pentachlorophenol, *J. Nanomater.*, **2014**,2014, 1-8.

[10] S. Kawasaki;K. Nakatsuji;J. Yoshinobu;F. Komori;R. Takahashi;M. Lippmaa;K. Mase;A. Kudo, Epitaxial Rh-doped SrTiO3 thin film photocathode for water splitting under visible light irradiation, *Appl. Phys. Lett.*, **2012**,101, 033910.

[11] R. Niishiro;R. Konta;H. Kato;W.-J. Chun;K. Asakura;A. Kudo, Photocatalytic O2 Evolution of Rhodium and Antimony-Codoped Rutile-Type TiO2 under Visible Light Irradiation, *J. Phys. Chem. C*, **2007**,111, 17420-17426.
[12] K. Iwashina;A. Kudo, Rh-Doped SrTiO3 Photocatalyst Electrode Showing Cathodic Photocurrent for Water Splitting under Visible-Light Irradiation, *J. Am. Chem. Soc.*, **2011**,133, 13272-13275.
[13] R. Abe;K. Shinmei;N. Koumura;K. Hara;B. Ohtani, Visible-Light-Induced Water Splitting Based on Two-Step Photoexcitation between Dye-Sensitized Layered Niobate and Tungsten Oxide Photocatalysts in the Presence of a Triiodide/Iodide Shuttle Redox Mediator, *J. Am. Chem. Soc.*, **2013**,135, 16872-16884.
[14] Q. Jia;A. Iwase;A. Kudo, $BiVO_4$-Ru/$SrTiO_3$:Rh composite Z-scheme photocatalyst for solar water splitting, *Chem. Sci.*, **2014**,5, 1513-1519.
[15] J. Kuncewicz;B. Ohtani, Titania photocatalysis through two-photon band-gap excitation with built-in rhodium redox mediator, *Chem. Commun.*, **2015**,51, 298-301.
[16] L. Zhao;X. Chen;X. Wang;Y. Zhang;W. Wei;Y. Sun;M. Antonietti;M.M. Titirici, One-step solvothermal synthesis of a carbon@TiO_2 dyade structure effectively promoting visible-light photocatalysis, *Adv. Mater.*, **2010**,22, 3317-3321.
[17] D. Dolat;S. Mozia;R.J. Wróbel;D. Moszyński;B. Ohtani;N. Guskos;A.W. Morawski, Nitrogen-doped, metal-modified rutile titanium dioxide as photocatalysts for water remediation, *Appl. Catal. B: Environ.*, **2015**,162, 310-318.
[18] D. Chu;A. Younis;S. Li, Direct growth of TiO_2 nanotubes on transparent substrates and their resistive switching characteristics, *J. Phys. D Appl. Phys.*, **2012**,45, 355306.
[19] L. Wang;X. Zhang;P. Zhang;Z. Cao;J. Hu, Photoelectric conversion performances of Mn doped TiO_2 under > 420 nm visible light irradiation, *J. Saudi Chem. Soc.*, **2015**,19, 595-601.
[20] R. Kobayashi;T. Takashima;S. Tanigawa;S. Takeuchi;B. Ohtani;H. Irie, A heterojunction photocatalyst composed of zinc rhodium oxide, single crystal-derived bismuth vanadium oxide, and silver for overall pure-water splitting under visible light up to 740 nm, *Phys. Chem. Chem. Phys.*, **2016**,18, 27754-27760.
[21] H. Kato;Y. Sasaki;N. Shirakura;A. Kudo, Synthesis of highly active rhodium-doped SrTiO3 powders in Z-scheme systems for visible-light-driven photocatalytic overall water splitting, *J. Mater. Chem. A*, **2013**,1, 12327-12333.
[22] R. Konta;T. Ishii;H. Kato;A. Kudo, Photocatalytic Activities of Noble Metal Ion Doped SrTiO3 under Visible Light Irradiation, *J. Phys. Chem. B*, **2004**,108, 8992-8995.
[23] K. Furuhashi;Q. Jia;A. Kudo;H. Onishi, Time-Resolved Infrared Absorption Study of SrTiO3 Photocatalysts Codoped with Rhodium and Antimony, *J. Phys. Chem. C*, **2013**,117, 19101-19106.
[24] Y. Okamoto;S. Ida;J. Hyodo;H. Hagiwara;T. Ishihara, Synthesis and Photocatalytic Activity of Rhodium-Doped Calcium Niobate Nanosheets for Hydrogen Production from a Water/Methanol System without Cocatalyst Loading, *J. Am. Chem. Soc.*, **2011**,133, 18034-18037.
[25] A.W. Morawski;E. Kusiak-Nejman;A. Wanag;J. Kapica-Kozar;R.J. Wróbel;B. Ohtani;M. Aksienionek;L. Lipińska, Photocatalytic degradation of acetic acid in the presence of visible light-active TiO_2 -reduced graphene oxide photocatalysts, *Catal. Today*, **2017**,280, 108-113.
[26] T. Torimoto;Y. Aburakawa;Y. Kawahara;S. Ikeda;B. Ohtani, Light intensity dependence of the action spectra of photocatalytic reactions with anatase titanium(IV) oxide, *Chem. Phys. Lett.*, **2004**,392, 220-224.
[27] B. Ohtani, Photocatalysis A to Z—What we know and what we do not know in a scientific sense, *J. Photochem. Photobiol. C: Photochem. Rev.*, **2010**,11, 157-178.

[28] S. Kawasaki;K. Akagi;K. Nakatsuji;S. Yamamoto;I. Matsuda;Y. Harada;J. Yoshinobu;F. Komori;R. Takahashi;M. Lippmaa;C. Sakai;H. Niwa;M. Oshima;K. Iwashina;A. Kudo, Elucidation of Rh-Induced In-Gap States of Rh:SrTiO3 Visible-Light-Driven Photocatalyst by Soft X-ray Spectroscopy and First-Principles Calculations, *J. Phys. Chem. C*, **2012**,116, 24445-24448.
[29] J. Kuncewicz;B. Ohtani, Rhodium-doped titania photocatalysts with two-step bandgap excitation by visible light-influence of the dopant concentration on photosensitization efficiency, *RSC Adv.*, **2016**,6, 77201-77211.
[30] Z. Wang;J. Hou;S. Jiao;K. Huang;H. Zhu, In situ chemical reduction of the Ta3N5 quantum dots coupled TaON hollow spheres heterojunction photocatalyst for water oxidation, *J. Mater. Chem.*, **2012**,22, 21972.
[31] K. Song;X. Han;G. Shao, Electronic properties of rutile TiO2 doped with 4d transition metals: First-principles study, *J. Alloy. Comp.*, **2013**,551, 118-124.
[32] F.E. Oropeza;R.G. Egdell, Control of valence states in Rh-doped TiO2 by Sb co-doping: A study by high resolution X-ray photoemission spectroscopy, *Chem. Phys. Lett.*, **2011**,515, 249-253.
[33] R. Wang;M.S. Shi;F.Y. Xu;Y. Qiu;P. Zhang;K.L. Shen;Q. Zhao;J.G. Yu;Y.F. Zhang, Graphdiyne-modified TiO2 nanofibers with osteoinductive and enhanced photocatalytic antibacterial activities to prevent implant infection, *Nat. Commun.*, **2020**,11, 12.

1 **Graphic abstract**

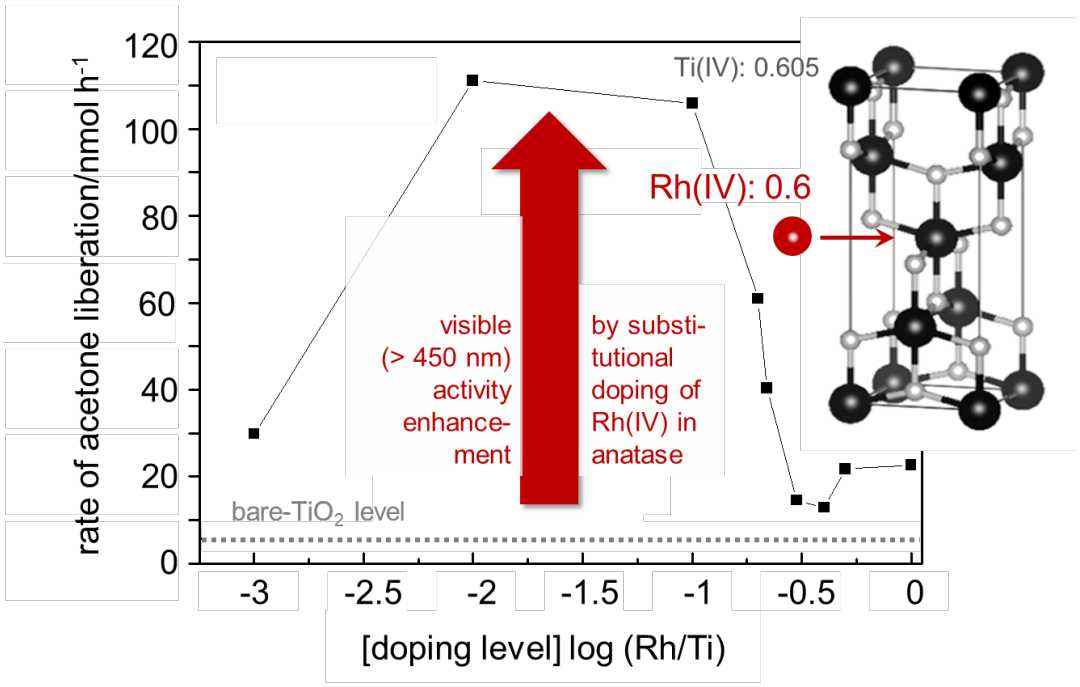

2

3

Highlights

- Titania directly doped with rhodium(IV) was successfully synthesized.
- Titanium(IV) is possibly substituted by rhodium(IV) in the crystalline lattice.
- The valence state of rhodium in the doped titania was studied.
- The enhanced activity is induced by rhodium(IV) doping.
- The enhancement is induced by a visible-light absorption.